





Article

Numerical Simulation and Performance Optimization of a Solar Cell Based on WO₃/CdTe Heterostructure Using NiO as HTL Layer by SCAPS 1D

José Carlos Zepeda Medina ¹, Enrique Rosendo Andrés ^{1,*}, Crisóforo Morales Ruíz ¹,
Eduardo Camacho Espinosa ², Leticia Treviño Yarce ³, Reina Galeazzi Isasmendi ¹, Román Romano Trujillo ¹,
Godofredo García Salgado ¹, Antonio Coyopol Solís ¹ and Fabiola Gabriela Nieto Caballero ⁴

- ¹ Posgrado en Dispositivos Semiconductores (PDS), Benemérita Universidad Autónoma de Puebla (BUAP), Av. San Claudio y 14 Sur, Edif. IC 5 C. U. Col. San Manuel, Puebla 72520, Mexico; jose.zepedam@alumno.buap.mx (J.C.Z.M.); crisoforo.morales@correo.buap.mx (C.M.R.); reina.galeazzi@correo.buap.mx (R.G.I.); roman.romano@correo.buap.mx (R.R.T.); godofredo.garcia@correo.buap.mx (G.G.S.); antonio.coyopol@correo.buap.mx (A.C.S.)
- ² Departamento de Física Aplicada, Centro de Investigación y de Estudios Avanzados del IPN Unidad Mérida, Km. 6, Antigua Carretera a Progreso, A. P. 73-Cordemex, Merida 97310, Mexico; eduardo.camacho@cinvestav.mx
- ³ Ingeniería en Energía, Universidad Politécnica de Amozoc, Av. Ampliación Luis Oropeza No. 5202, San Andrés las Vegas 1ra Sección, Amozoc de Mota 72980, Mexico; leticia.trevino@upamozoc.edu.mx
- ⁴ Facultad de Ciencias Químicas (FCQ), Benemérita Universidad Autónoma de Puebla (BUAP), Av. San Claudio y 18 Sur, Edif. FCQ 1 C. U. Col. San Manuel, Puebla 72520, Mexico; fabiola.nieto@correo.buap.mx
- * Correspondence: enrique.rosendo@correo.buap.mx



Citation: Medina, J.C.Z.; Andrés, E.R.; Ruíz, C.M.; Espinosa, E.C.; Yarce, L.T.; Galeazzi Isasmendi, R.; Trujillo, R.R.; Salgado, G.G.; Solís, A.C.; Caballero, F.G.N. Numerical Simulation and Performance Optimization of a Solar Cell Based on WO₃/CdTe Heterostructure Using NiO as HTL Layer by SCAPS 1D. *Coatings* **2023**, *13*, 1436. <https://doi.org/10.3390/coatings13081436>

Academic Editors: Qi Hua Fan and Alessandro Latini

Received: 30 June 2023

Revised: 26 July 2023

Accepted: 10 August 2023

Published: 15 August 2023



Copyright: © 2023 by the authors. Licensee MDPI, Basel, Switzerland. This article is an open access article distributed under the terms and conditions of the Creative Commons Attribution (CC BY) license (<https://creativecommons.org/licenses/by/4.0/>).

Abstract: In this paper, a solar cell based on WO₃/CdTe heterojunction was analyzed and optimized, for which the following structure of the Al/AZO/WO₃/CdTe/NiO/Ni device was proposed, which was numerically simulated by the SCAPS 1-D software. Using the software, the effect of the thickness and carrier concentration of the absorber layer (CdTe) and the window layer (WO₃) was analyzed, and the optimal value of these parameters was found to be 2 μm and 10¹⁵ cm⁻³ for the CdTe layer and 10 nm and 10¹⁹ cm⁻³ for the WO₃ layer, respectively. The influence of the defect density of the WO₃/CdTe interface on the performance of the proposed cell was also analyzed, simulating from 10¹⁰ to 10¹⁶ cm⁻², obtaining better device performance at lower interface defect density. Another parameter analyzed was the operating temperature on the photovoltaic performance of the device, observing that the solar cell has a better performance at lower temperatures. Finally, a maximum optimized PCE of 19.87% is obtained with a V_{oc} = 0.85 V, J_{sc} = 28.45 mA/cm², and FF = 82.03%, which makes the WO₃/CdTe heterojunction an interesting alternative for the development of CdTe-based solar cells.

Keywords: CdTe thin film; WO₃ window layer; SCAPS-1D; WO₃/CdTe; solar cell performance optimization

1. Introduction

CdTe is a p-type semiconductor material with a band gap of ~1.49 eV [1] and an absorption coefficient of ~10⁵ cm⁻¹, which allows it to absorb more than 99% of the incident photons with an energy greater than its band gap in films as thin as ~2 μm [2]. In addition, CdTe can be produced on a large scale with good cost efficiency due to its adaptability to manufacturing processes [3]. These characteristics allow considering CdTe as a suitable material for the development of thin-film solar cells.

Generally, a CdTe thin-film solar cell is manufactured in a superstrate configuration, with a glass/TCO/CdS/CdTe/Back contact structure [4]. CdTe is the absorbing part of the

cell where the most carrier generation and accumulation take place. In order to improve the efficiency of solar cells based on this heterojunction, alternatives are being used in cell architecture that incorporates nanostructured materials, such as the case of Di Carlo V. et al. [5], who report the growth of CdTe nanowires with a gap energy of 1.539 eV. Meanwhile, Hongmei Dang et al. [6] report the fabrication and characterization of a solar cell based on the CdS nanowires/CdTe heterojunction and found substantial improvements.

The CdS, with a bandgap of ~ 2.4 eV, is a good choice as a window layer, since it allows most of the incident photons of sunlight to pass through it. Until now, it has been the most widely used semiconductor to form the pn junction together with CdTe to carry out the photovoltaic effect [7]. However, due to its energy bandgap, photons whose energy is above this energy bandgap value are absorbed by it, and the photogenerated carriers in this layer are not collected, generating a parasitic absorption that harms the short-circuit current density (J_{sc}) [2,8].

For its part, ZnO:Al is an ideal candidate to be used as a transparent conductive oxide (TCO), since it has a wide band gap (3.3 eV) and excellent optical and electrical properties [9], in addition to being abundant materials in nature.

Along with the experimental work, in recent years, simulations of solar cells have been carried out, which has made it possible to optimize the time and cost of the experimental processes, as in the case reported by Montoya de los Santos et al. [10], who report a theoretical increase in the efficiency of a solar cell based on the CdS/CdTe heterojunction using ZnO:Al and CuSCN nanolayers.

On the other hand, WO_3 is a chemically stable n-type semiconductor material with a wide band gap of ~ 3.15 eV [11], it can present different crystallographic phases depending on the synthesis temperature: tetragonal, orthorhombic, and monoclinic. WO_3 is a non-toxic, low-cost, and easily evaporable material and is generally used as an ETL layer in solar cell design [12].

With the aim of seeking alternatives, in this paper, we propose to introduce WO_3 to replace CdS as a window layer due to its low toxicity and wide band gap, seeking to reduce the absorption of incident photons in the window layer and thus study the feasibility of a substrate-type solar cell at CdTe base performing a heterojunction with WO_3 as layer n. Figure 1 shows the quantum efficiency (QE) of simulated CdS/CdTe and WO_3 /CdTe heterojunctions, where it can be seen that when using WO_3 as a window layer, a QE of practically 100% is obtained at wavelengths of 300–520 nm. When using CdS as a window layer, there is a reduction in the simulated QE due to the band gap of the CdS, decreasing to 90% at wavelengths corresponding to incident photons with energy greater than 2.4 eV. The results obtained in this study reflect that using WO_3 as a window layer reduces parasitic absorption in this layer, obtaining a higher J_{sc} than when using CdS as a window layer, as reported in the following investigations: 23 mA/cm² [3], 24.18 mA/cm² [13], 23.75 mA/cm² [14], and 25.5 mA/cm² [15].

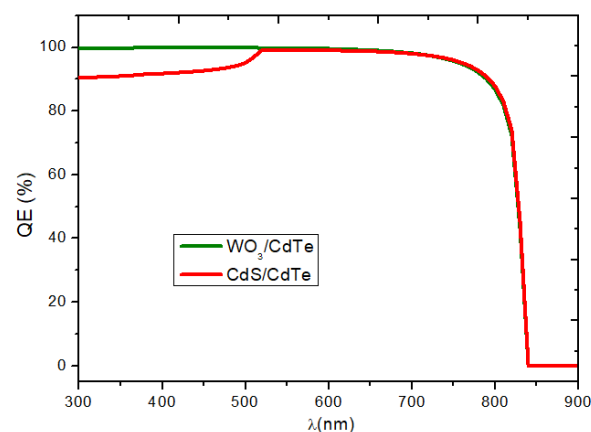


Figure 1. Simulated quantum efficiency for CdS/CdTe and WO_3 /CdTe heterojunctions.

In this study, the effect of varying the thickness and carrier concentration of the CdTe layer and WO_3 , as well as the effect of defect density at the WO_3/CdTe interface was simulated and analyzed on the device's photovoltaic performance, and the operating temperature using SCAPS 1-D software. Said analysis was carried out through the main photovoltaic parameters: open circuit voltage (V_{oc}), short-circuit current density (J_{sc}), fill factor (FF), and efficiency (PCE) under standard lighting (AM 1.5 G 1000 W/m^2 , 300 K).

2. Device Modeling and Simulation

2.1. Numerical Method

A numerical simulation is a tool that allows us to understand and analyze the influence of different physical parameters on the performance of a solar cell, which allows us to analyze and optimize different structures of solar cells based on crystalline, polycrystalline, and amorphous materials [16], minimizing the cost and time of manufacturing prototypes. SCAPS 1-D, being a software intended for the simulation of semiconductor material properties, allows us to analyze the influence of each layer that makes up the structure of the solar cell to be simulated.

Simulator of the capacitance of solar cells-1 dimension (SCAPS-1D) is a numerical modeling software designed to simulate the DC and AC electrical characteristics of thin-film heterojunction solar cells and has been specially developed for $\text{Cu}(\text{In,Ga})\text{Se}_2$ and CdTe solar cells [16].

The working principle of SCAPS-1D is based on Poisson's equations, steady-state electron-hole continuity and the electron and hole current densities [17].

$$\frac{\partial^2 \psi(x)}{\partial x^2} + \frac{q}{\epsilon_r \epsilon_0} [p(x) - n(x) + N_D^+(x) - N_A^-(x) + p_t(x) - n_t(x)] = 0 \quad (1)$$

where ψ is the electrostatic potential; N_D^+ is the ionized donor concentration; N_A^- is the ionized acceptor density; n and p are, respectively, hole and electron density; ϵ_r and ϵ_0 are, respectively, relative and vacuum permittivity; p_t and n_t represent the holes and electrons trapped, respectively; q is the electron charge; and x is the position in the x -coordinate.

$$-\frac{\partial J_n}{\partial x} + G - R = 0 \quad (2)$$

$$-\frac{\partial J_p}{\partial x} + G - R = 0 \quad (3)$$

G is the carrier generation rate, R is the net recombination from direct and indirect band, and J_p and J_n are, respectively, hole and electron current densities

$$J_n = qn\mu_n E + qD_n \frac{\partial n}{\partial x} \quad (4)$$

$$J_p = qp\mu_p E - qD_p \frac{\partial p}{\partial x} \quad (5)$$

D_p and D_n are, respectively, hole and electron diffusion coefficients; E is the electric field; and μ_p and μ_n are, respectively, hole and electron mobilities. In this research work, software version 3.3.10 was used.

2.2. Device Structure and Simulation Parameters

Figure 2 shows the structure of the simulated device, at the top of the aluminum front contact, with AZO as transparent conductive oxide (TCO), the n-type layer or window layer of WO_3 , the CdTe absorber layer, a hole transporter layer (HTL) of NiO, and Ni as back contact at the bottom of the device. Due to the high work function of CdTe ($\sim 5.5 \text{ eV}$) [2], a metal with a higher work function than CdTe is required to achieve an ohmic contact, so NiO was incorporated as an HTL layer between the CdTe absorber layer and the Ni back

contact. The high concentration of acceptor carriers and work function (~5.2 eV) of NiO help to extract the carrier from the back contact, improving the quality of the ohmic contact.

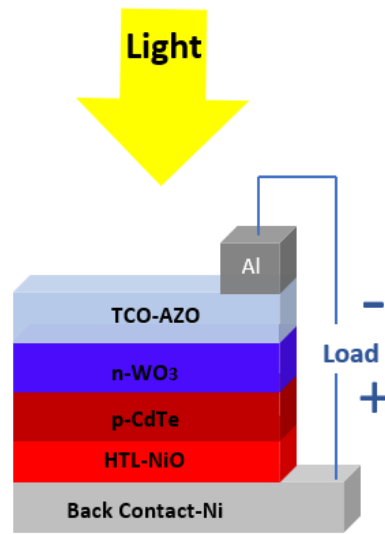


Figure 2. Schematic representation of the simulated device (Al/AZO/WO₃/CdTe/NiO/Ni).

Figure 3a shows the energy band diagram of the simulated structure using WO₃ as a window layer the difference between the conduction and valence bands between the CdTe and WO₃ layers are $\Delta E_c = 0.27$ eV and $\Delta E_v = 1.93$ eV, respectively. The thickness of the depletion zone (W) is 0.731 μm . The power barrier V_{bi} is 1.03 V. The Fermi level for CdTe and WO₃ with respect to the valence band is 0.195 and 3.14 eV, respectively. The work function of CdTe is 5.5 eV, while the work function of WO₃ is 4.5 eV. Figure 3b shows the band diagram using CdS as a window layer, where we have an $\Delta E_c = 0.38$ eV, $\Delta E_v = 0.55$ eV, $V_{bi} = 1.32$ V, and $W = 0.817$ μm . It can also be seen that using WO₃ as a window layer does not generate a peak in the conduction band because WO₃ has a higher electron affinity than CdTe, favoring transport by diffusion. On the other hand, when using CdS as a window layer, a peak is generated in the conduction band, which limits the transport of electrons by diffusion from the n region to the p region, having as the dominant transport mechanism, potential barrier overcoming, tunneling and recombination at the interface. The work function of CdS is ~4 eV, so to have an ohmic contact with this material, a metal with a work function of less than 4 eV is needed. However, given the work function of WO₃, it allows us to obtain an ohmic contact when using metals like Al and Ag as front contacts.

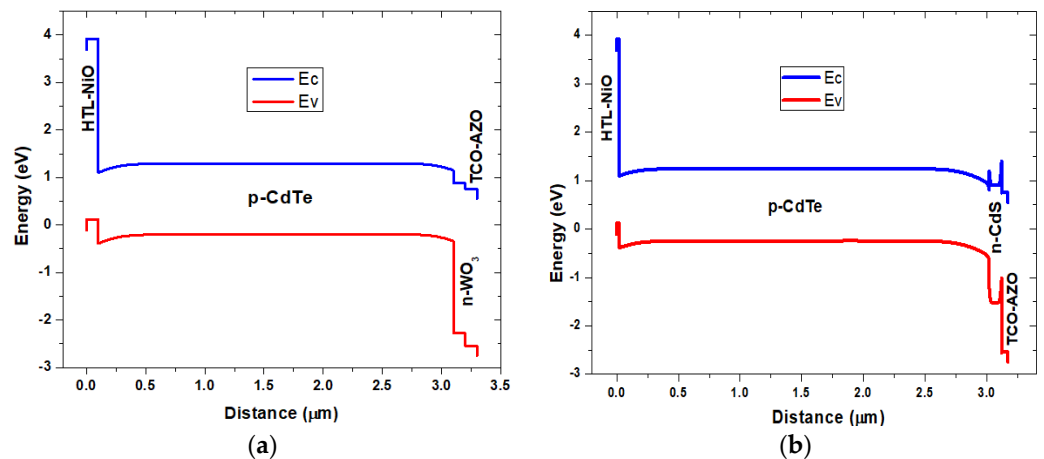


Figure 3. Energy band diagram of the simulated devices: (a) (Al/AZO/WO₃/CdTe/NiO/Ni) and (b) (Al/AZO/CdS/CdTe/NiO/Ni).

To carry out the simulation process, the SCAPS-1D software requires the input of physical parameters of the layers that make up the device to be simulated (Figure 2), which are described in Table 1. SCAPS-1D also allows the electrical properties of the back and front contacts to be incorporated into the simulation process, as well as the defect density (N_t) of the WO_3/CdTe interface (Table 2), which are generated by the network mismatch between both layers, promoting free links that favor the appearance of recombination centers [18].

Table 1. Parameters used in the simulation of the structure Al/AZO/ WO_3 /CdTe/NiO/Ni.

Parameters	CdTe [1]	WO_3 [12,18,19]	NiO [1,20]	AZO [20,21]
Thickness (μm)	0.5–3	0.01–0.15	0.020	0.050
Bandgap, E_g (eV)	1.49	3.15	3.8	3.3
Electron Affinity, x (eV)	4.28	4.55	1.46	4.55
Relative permittivity, ϵ_r	9.4	10	10	8.12
Effective CB density of states, N_c (cm^{-3})	8×10^{17}	4.2×10^{18}	2.8×10^{19}	4.1×10^{18}
Effective VB density of states, N_v (cm^{-3})	1.8×10^{19}	9×10^{18}	1×10^{19}	8.2×10^{18}
Electron mobility, μ_n (cm^2/Vs)	500	20	12	100
Hole mobility, μ_p (cm^2/Vs)	60	10	2.8	20
Electron Thermal Velocity (cm/s)	10^7	10^7	10^7	2.2×10^7
Hole Thermal Velocity (cm/s)	10^7	10^7	10^7	1.5×10^7
Donor concentration, N_D (cm^{-3})	0	10^{13} – 10^{19}	0	10^{21}
Acceptor concentration, N_A (cm^{-3})	10^{13} – 10^{17}	0	10^{21}	0
Defect density, N_t ($1/\text{cm}^3$)	10^{15}	10^{12}	10^{14}	5×10^{14}
Defect type	acceptor	donor	acceptor	acceptor

Table 2. Simulation Parameters for Interface Defects and Contacts.

<i>Interface Defect Density [12,19]</i>		-
WO_3/CdTe		10^{10} – 10^{16} cm^{-2}
Defect type		Acceptor
Capture cross-section electrons/holes		10^{-15} cm^{-2}
<i>Back Contact Electrical Properties [22,23]</i>		-
Work function of Ni		5.15 eV
Surface recombination velocity of electrons		10^5 cm/s
Surface recombination velocity of holes		10^7 cm/s
<i>Front Contact Electrical Properties [22,23]</i>		-
Work function of Al		4.2 eV
Surface recombination velocity of electrons		10^7 cm/s
Surface recombination velocity of holes		10^5 cm/s

Regarding the working conditions of the simulation, it was performed with AM 1.5 G standard illumination and a temperature of 300 K, except in the section where these parameters are discussed. A default mesh of 51 points with a step size of 0.02 V was used for the I-V analysis since the SCAPS-1D algorithm is designed in such a way that it provides a larger number of points in the mesh in regions where the materials properties experience a greater variation (near interfaces/contacts), but in areas where the properties are expected to remain practically constant (in the bulk), the algorithm provides fewer points for the discretization of the mesh [17]. SCAPS-1D allows an increase or decrease in the number of points to optimize the mesh; however, in this investigation, we work with the number of points in the mesh predetermined by the software because when increasing or decreasing the number of points in the mesh, there were practically no changes in the results obtained.

3. Results and Discussion

3.1. Effect of the Thickness and Concentration of Carriers (N_D) of the Window Layer WO_3

To analyze the effect of the thickness and concentration of carriers (N_D) of the window layer WO_3 on the performance of the devices, these were varied from 10 to 150 nm and from 10^{13} to 10^{19} cm^{-3} , respectively. The other parameters were kept constant during the simulation.

In Figure 4a, it can be seen that J_{sc} decreases from 28.45 to 28.33 mA/cm^2 when the thickness of the window layer increases from 10 to 150 nm, since having a greater thickness in this layer favors a greater absorption of the incident photons, transmitting fewer photons to the absorbing CdTe layer and thus decreasing J_{sc} . V_{oc} remains practically constant (Figure 4a) as the thickness of the window layer increases since the carrier diffusion length allows the carriers separated by the electric field generated by the pn junction to reach frontal contact, thus maintaining the separation of charges. FF has a small decrease when the window layer's thickness increases, going from 81.95 to 81.13%. Since J_{sc} and FF decrease, PCE also decreases (Equation (6)) with increasing window layer thickness, decreasing from 19.87 to 18.97% (Figure 4a).

$$PCE = \frac{J_{sc} V_{oc} FF}{P_{in}} \tag{6}$$

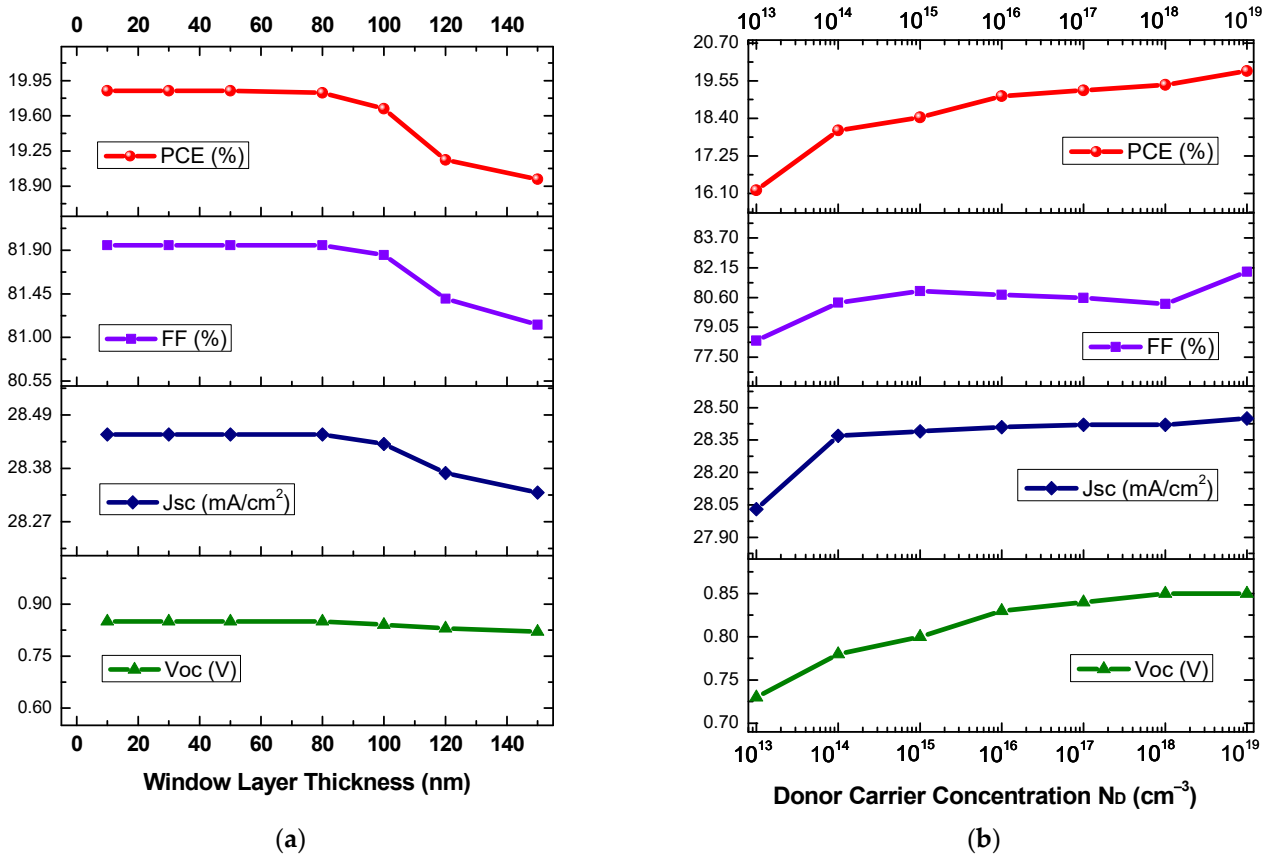


Figure 4. Change in V_{oc} , J_{sc} , FF , and PCE for different (a) thicknesses and (b) concentrations of N_D carriers in the window layer.

Figure 4b shows the behavior of V_{oc} , which increases from 0.73 to 0.85 V by increasing N_D from 10^{13} to 10^{19} cm^{-3} because the depletion zone increases on the side of the absorber layer by increasing N_D , which favors a greater generation and separation of photogenerated carriers. J_{sc} increases from 28.03 to 28.46 mA/cm^2 when N_D increases from 10^{13} to 10^{19} cm^{-3} (Figure 4b). This is also due to the increase in the depletion zone in the absorber layer as N_D increases, favoring an increase in the number of photogenerated carriers collected

by the contacts. FF increases from 78.36 to 81.95% (Figure 4b) when N_D increases from 10^{13} to 10^{19} cm^{-3} . This is due (Equation (7)) to the fact that the maximum cell voltage (V_m) increases from 0.64 to 0.75 V generating that the maximum power (P_m) of the simulated device increases with the increase in N_D . In the same figure, the PCE increases as N_D increases, going from 16.20 to 19.87%, since the photogenerated electrons in the absorber layer will have a higher probability of passing through the junction and being collected by the frontal contact.

$$FF = \frac{P_m}{V_{oc}J_{sc}} \quad (7)$$

3.2. Effect of the Thickness and Acceptor Carrier Concentration (N_A) in CdTe Absorber Layer

In this section, the effect of the thickness and carrier concentration (N_A) in the CdTe absorber layer was studied, for which the thickness of the CdTe layer was varied from 0.5 to 3 μm , while the carrier's concentration was varied from 10^{13} to 10^{17} cm^{-3} . The other parameters were kept constant during the simulation.

In Figure 5a, it can be seen that J_{sc} has a value of 25.80 mA/cm^2 at a thickness of 0.5 μm , reaching a maximum value of 28.45 mA/cm^2 from 2 μm , since having a thicker film has a higher absorption [2] because the probability that the photons are absorbed is higher due to a longer optical path. The behavior of V_{oc} remains practically constant when varying the thickness of the absorbent layer, having a negligible decrease in V_{oc} of 0.01 V as the thickness increases from 0.5 to 1 μm . This behavior can be explained by the fact that (Equation (8)) J_{sc} remains constant from 1.5 μm , and the saturation current density (J_0) is not affected by the increase in the thickness of the absorber layer. Since FF is inversely proportional (Equation (7)) to J_{sc} and V_{oc} , and since there is a greater increase in J_{sc} compared to the decrease in V_{oc} when increasing the thickness of the absorber layer, FF decreases from 85.78 to 81.97% when increasing the thickness of the absorbent layer from 0.5 to 3 μm (Figure 5a). PCE increases from 19.02 to 19.87% when the thickness of the absorber layer increases since there is a greater generation of electron-hole pairs given by a greater absorption capacity by having a thicker CdTe layer.

$$V_{oc} = \frac{kT}{q} \ln \left(\frac{J_{sc}}{J_0} + 1 \right) \quad (8)$$

Figure 5b shows the behavior of J_{sc} as a function of the concentration of N_A carriers in the absorber layer, which increases from 21.38 to 28.45 mA/cm^2 as N_A increases from 10^{13} to 10^{15} cm^{-3} since having a higher concentration of carriers improves the conductivity of the material, thus favoring a better extraction of the carrier from the back contact; however, J_{sc} decreases when exceeding a N_A of 10^{15} cm^{-3} , decreasing its value to 24.57 mA/cm^2 with a N_A of 10^{17} cm^{-3} , since the fermi level of the holes on the p side decreases, thus increasing the power barrier V_{bi} making it difficult for carriers to flow through the junction. V_{oc} decreases from 1.12 to 0.93 V when N_A increases from 10^{13} to 10^{17} cm^{-3} . This is because the mobility of the carriers decreases when N_A increases [24], which reduces the diffusion length of the carrier (L_n) and the equilibrium electron density on the p side (n_{p0}) thus increasing an increase in the saturation current J_0 (Equation (9)).

$$J_0 = \frac{qD_p p_{n0}}{L_p} + \frac{qD_n n_{p0}}{L_n} \quad (9)$$

FF increases from 33.97 to 82.03% (Figure 5b) by increasing N_A from 10^{13} to 10^{15} cm^{-3} mainly due to the behavior of V_{oc} (Equation (7)); however, by increasing N_A to 10^{17} cm^{-3} , FF decreases to 76.74% mainly due to the maximum current density of the device (J_m) decreasing from 26.44 to 21.68 mA/cm^2 , causing P_m to decrease, for which FF decreases (Equation (7)). PCE has its maximum value of 19.87% at a N_A of 10^{15} cm^{-3} due to the increase in J_{sc} and FF; however, PCE decreases when N_A exceeds 10^{15} cm^{-3} . This is due to the decrease in J_{sc} and FF.

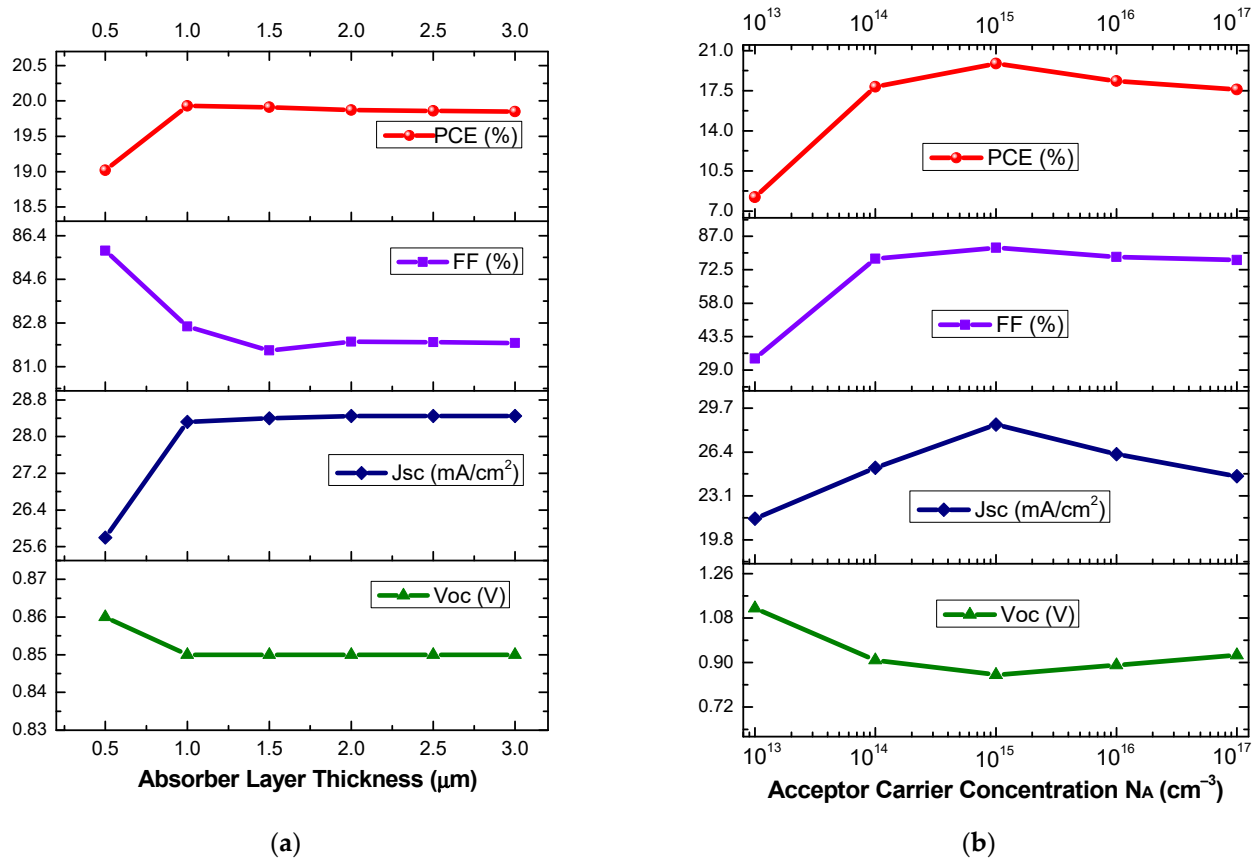


Figure 5. Change in V_{oc} , J_{sc} , FF , and PCE for different (a) thicknesses and (b) concentrations of N_A carriers in the absorber layer.

3.3. Effect of Defect Density (N_t) at the $WO_3/CdTe$ Interface

To understand the effect of the density of states of the $WO_3/CdTe$ interface, it was varied from 10^{10} to 10^{16} cm^{-2} , the other parameters were kept constant during the simulation. Figure 6 shows that the performance of the solar cell is negatively affected by a higher defect density in the interface. V_{oc} is the one that has a greater decrease when increasing the density of defects in the interface, decreasing from 0.85 to 0.60 V, since having a greater density of defects has a greater number of recombination centers [18], which generates that the probability that the photogenerated carriers are separated is lower. J_{sc} has a decrease of 0.26 mA/cm^2 with increasing defect density from 10^{10} to 10^{16} cm^{-2} . By increasing N_t , there is a greater probability that the photogenerated carriers recombine at the junction interface, causing V_m to decrease from 0.75 to 0.51 V, therefore the maximum power (P_m) of the cell decreases and, consequently FF decreases (Equation (7)) from 82.03 to 77.93% even if J_{sc} and V_{oc} decrease. PCE decreases from 19.87 to 13.27% as N_t increases, mainly due to the decrease in V_{oc} .

3.4. Effect of Operating Temperature

To study the behavior of the solar cell depending on the temperature to which it will be subjected. This was varied from 270 to 370 K since the solar cells in their applications can be exposed to this temperature range outdoors. The other parameters analyzed were kept constant at their optimized values.

Being more specific, V_{oc} decreases by 0.15 V when the operating temperature increases by 100 K, as can be seen in Figure 7d. This behavior may be due to the fact that, as the temperature increases the density of carriers increases, which reduces their mobility as observed in Equation (8), thus increasing J_0 and consequently decreasing V_{oc} (Equation (8)). J_{sc} has a practically constant behavior when increasing the temperature from 270 to 370 K

(Figure 7c). Figure 7b shows that FF has a small decrease of 0.73% when the operating temperature increases by 100 K, due to the behavior of V_{oc} and to the fact that V_m decreases from 0.77 to 0.62 V with increasing temperature. In Figure 7a, it can be seen that PCE decreases from 20.27 to 16.82% when the temperature increases by 100 K, given that when the temperature of a material is increased, its conductivity is affected and that phonons are generated [23], which cause scattering in charge carriers thus affecting PCE .

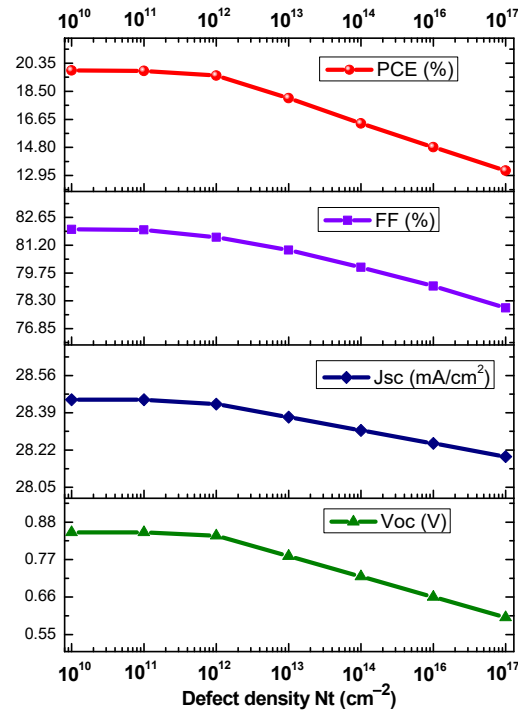


Figure 6. Effect of defect density at the WO_3/CdTe interface on V_{oc} , J_{sc} , FF , and PCE .

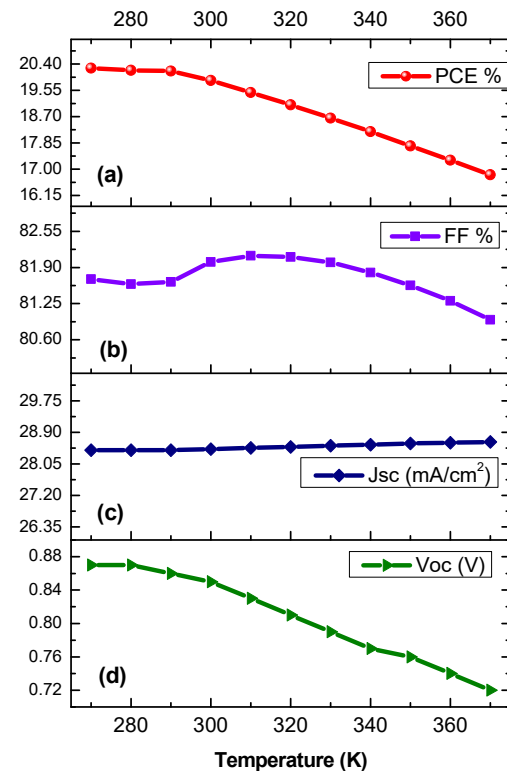


Figure 7. Effect of operating temperature on (a) V_{oc} , (b) J_{sc} , (c) FF , and (d) PCE .

4. Conclusions

In this paper, we simulate and analyze the photovoltaic performance of a CdTe-based solar cell using WO_3 as a window layer, with a device structure of Al/AZO/ WO_3 /CdTe/NiO/Ni, using the SCAPS 1-D software. It was found that the concentration of N_A carriers in the absorber layer plays an important role in the solar cell's performance, obtaining the maximum PCE at a N_A of 10^{15} cm^{-3} . It was also observed that the photovoltaic performance of the simulated solar cell has an almost constant behavior from 1.5 μm thick on the absorber layer. As the thickness of the window layer increases, PCE decreases; however, it is not such a determining factor for the photovoltaic performance of the cell. On the other hand, the concentration of N_D carriers of the window layer is a very determining factor, obtaining a maximum PCE at a N_D of 10^{19} cm^{-3} . The increase in the density of N_t defects at the WO_3 /CdTe interface negatively affects PCE, decreasing by 6.60% when increasing N_t from 10^{10} to 10^{16} cm^{-2} . The solar cell's performance is impaired with the increase in operating temperature, since at lower temperatures, a higher efficiency is obtained, such that at 270 K, a PCE of 20.27% is obtained. PCE decreases by 3.45% as the operating temperature increases until 370 K, having an acceptable performance at extreme temperatures. The other sections were simulated at standard temperatures of 300 K.

A maximum PCE of 19.87% was obtained with a $V_{oc} = 0.85 \text{ V}$, $J_{sc} = 28.45 \text{ mA/cm}^2$, and $FF = 82.03\%$, achieved with a thickness and carrier concentration of 2 μm and 10^{15} cm^{-3} , respectively, for the absorber layer and the window layer a thickness of 10 nm and a carrier concentration of 10^{19} cm^{-3} . CdS remains theoretically and experimentally one of the best options to be used as a window layer in heterojunction with CdTe; however, based on the results obtained in this research, WO_3 has the potential to become a viable alternative as a window layer for the development of CdTe-based solar cells, since it can favor the increase in J_{sc} due to its wide band gap, in addition to being a non-toxic and low-cost material.

Author Contributions: Conceptualization, J.C.Z.M.; Data curation, G.G.S.; Formal analysis, J.C.Z.M. and E.R.A.; Investigation, J.C.Z.M.; Methodology, J.C.Z.M. and E.R.A.; Resources, R.G.I. and R.R.T.; Software, J.C.Z.M.; Supervision, E.R.A.; Validation, C.M.R., E.C.E. and L.T.Y.; Visualization, A.C.S. and F.G.N.C.; Writing—original draft preparation, J.C.Z.M. and E.R.A.; Writing—review and editing, J.C.Z.M. All authors have read and agreed to the published version of the manuscript.

Funding: This research received no external funding.

Institutional Review Board Statement: Not applicable.

Informed Consent Statement: Not applicable.

Data Availability Statement: Data will be made available on request.

Acknowledgments: Jose Carlos Zepeda Medina is grateful for the scholarship CONACYT #1028131. The authors also appreciate the support granted by the BUAP to carry out this research.

Conflicts of Interest: The authors declare no conflict of interest.

References

1. Zepeda, J.C.; Rosendo, E.; Morales, C.; Camacho, E. Performance simulation of solar cell based on AZO/CdTe heterostructure by SCAPS 1D software. *Heliyon* **2023**, *9*, e14547. [[CrossRef](#)]
2. Camacho, E. Caracterización de Películas Policristalinas de CdTe, Obtenidas por Erosión Catódica para su Aplicación en Celdas Solares. Ph.D. Thesis, BUAP, Puebla, Mexico, 2014.
3. Bhari, B.Z.; Rahman, K.S.; Chelvanathan, P.; Ibrahim, M.A. Numerical Simulation of Ultrathin CdTe Solar Cell by SCAPS-1D. *IOP Conf. Ser. Mater. Sci. Eng.* **2023**, *1278*, 012002. [[CrossRef](#)]
4. Yang, R.; Wang, D.; Wan, L.; Wang, D. High efficiency CdTe thin film solar cell with a mono-grained CdS window layer. *RSC Adv.* **2014**, *4*, 22162–22171. [[CrossRef](#)]
5. Di Carlo, V.; Prete, P.; Dubrovskii, V.G.; Berdnikov, Y.; Lovergine, N. CdTe Nanowires by Au-catalyzed metalorganic vapor phase epitaxy. *Nano Lett.* **2017**, *17*, 4075–4082. [[CrossRef](#)]
6. Dang, H.; Ososanaya, E.; Zhang, N. Improving reliability of window-absorber solar cells through CdS nanowires. *Opt. Mater.* **2022**, *132*, 112721. [[CrossRef](#)]
7. Lovergine, N.; Cingolani, R.; Mancini, A.M. Photoluminescence of CVD grown CdS Epilayers on CdTe substrates. *J. Crystal Growth* **1992**, *118*, 304–308. [[CrossRef](#)]

8. Colegrove, R.; Banai, C.; Blissett, C.; Buurma, J. Ellsworth, High-efficiency polycrystalline CdS/CdTe solar cell buffered commercial TCO-coated glass. *J. Electron. Mater.* **2012**, *41*, 2833–2837. [[CrossRef](#)]
9. Miccoli, I.; Spampinato, R.; Marzo, F.; Prete, P.; Lovergine, N. DC-magnetron sputtering of ZnO:Al films on (00.1)Al₂O₃ substrates from slip-casting sintered ceramic targets. *Appl. Surf. Sci.* **2014**, *313*, 418–423. [[CrossRef](#)]
10. Montoya De Los Santos, I.; Pérez-Orozco, A.A.; Liña-Martínez, D.A.; Courel, M.; Meza-Avendaño, C.A.; Borrego-Pérez, J.A.; Pérez, L.M.; Laroze, D. Towards a CdTe Solar Cell Efficiency Promotion: The Role of ZnO:Al and CuSCN Nanolayers. *Nanomaterials* **2023**, *13*, 1335. [[CrossRef](#)]
11. Mahjabin, S.; Haque, M.; Sobayel, K.; Jamal, M.S. Perceiving of Defect Tolerance in Perovskite Absorber Layer for Efficient Perovskite Solar Cell. *IEEE Access* **2020**, *8*, 106346–106353. [[CrossRef](#)]
12. Karimi, E.; Dabbagh, G.R.; Ghorashi, S.M.; Nekuee, F. Electrical Simulation of the Function of Tungsten Oxide in Polymeric Solar Cells. *Mater. Res. Express* **2019**, *6*, 126335. [[CrossRef](#)]
13. Mekky, A. Simulation and modeling of the influence of temperature on CdS/CdTe thin film solar cell. *Eur. Phys. J. Appl. Phys.* **2019**, *87*, 30101. [[CrossRef](#)]
14. Nykyruy, L.I.; Yavorskyi, R.S.; Zapukhlyak, Z.R.; Wisz, G. Evaluation of CdS/CdTe thin film solar cells: SCAPS thickness simulation and analysis of optical properties. *Opt. Mater.* **2019**, *92*, 319–329. [[CrossRef](#)]
15. Teloeken, A.C.; Lamb, D.A.; Dunlop, T.O.; Irvine, S.J.C. Effect of bending test on the performance of CdTe solar cells on flexible ultra-thin glass produced by MOCVD. *Sol. Energy Mater. Sol. Cells* **2020**, *211*, 110552. [[CrossRef](#)]
16. Burgelman, M.; Nollet, P.; Degraeve, S. Modelling polycrystalline semiconductor solar cells. *Thin Solid Films* **2000**, *361*, 527–532. [[CrossRef](#)]
17. Burgelman, M.; Decock, K. *SCAPS Manual*; University of Gent: Gent, Belgium, 2020.
18. Li, D.B.; Song, Z.; Awni, R.; Sandip, S.; Niraj, S.; Corey, R. Eliminating S-kink to maximize the performance of MgZnO/CdTe solar cells. *ACS Appl. Energy Mater.* **2019**, *2*, 2896–2903. [[CrossRef](#)]
19. Otoufi, M.K.; Ranjbar, M.; Kermanpur, A.; Taghavinia, N. Enhanced performance of planar perovskite solar cells using TiO₂/SnO₂ and TiO₂/WO₃ bilayer structures: Roles of the interfacial layers. *Sol. Energy* **2020**, *20*, 697–707. [[CrossRef](#)]
20. Abdelkadir, A.A.; Oublal, E.; Sahal, M.; Gibaud, A. Numerical simulation and optimization of n-Al-ZnO/n-CdS/p-CZTSe/p-NiO (HTL)/Mo solar cell system using SCAPS-1D. *Results Opt.* **2022**, *8*, 100257. [[CrossRef](#)]
21. Mora, D.; Pal, M.; Santos, J. Theoretical modelling and device structure engineering of kesterite solar cells to boost the conversion efficiency over 20%. *Sol. Energy* **2021**, *220*, 316–330. [[CrossRef](#)]
22. Abdy, H.; Aletayeb, A.; Kolahdouz, M.; Soleimani, E.A. Investigation of metal-nickel oxide contacts used for perovskite solar cell. *AIP Adv.* **2019**, *9*, 015216. [[CrossRef](#)]
23. Rahman, M.A. Design and simulation of high-performance Cd-free Cu₂SnSe₃ solar cells with SnS electron-blocking hole transport layer and TiO₂ electron transport layer by SCAPS-1D. *SN Appl. Sci.* **2021**, *3*, 253. [[CrossRef](#)]
24. Colinge, J.P. *Physics of Semiconductor Devices*; Kluwer Academic Publisher: Amsterdam, The Netherlands; University of California: Los Angeles, CA, USA, 2002; p. 54.

Disclaimer/Publisher’s Note: The statements, opinions and data contained in all publications are solely those of the individual author(s) and contributor(s) and not of MDPI and/or the editor(s). MDPI and/or the editor(s) disclaim responsibility for any injury to people or property resulting from any ideas, methods, instructions or products referred to in the content.